they substantially changed when the number of days included per month in the analysis is increased from 1 to 10. When this number of days is increased above 15, the ozone trends systematically revert to the expected climatological mean (0.5%/year). The trend in UV radiation decreases more rapidly because in the early years, when data were not taken during inclement weather conditions, the measurements were systematically biased toward higher values. These sampling differences would also bias any attempts to infer long-term changes in mean values from the current data set. For the purpose of assessing risks to humans, a consideration of peak midday values is perhaps more relevant, because the population is less likely to be exposed to UV radiation during inclement weather.

Because the downward trends in ozone had already been occurring for several years before the UV radiation measurements became available, one could infer that even larger increases in UV radiation may have accrued at this site since 1979. The future outlook is more uncertain. Although the stratospheric loading of ozone-depleting substances is now close to the maximum expected under the present control regime (*3*), there is concern about possible interactions between ozone depletion and global warming, which could delay the recovery of ozone by decades (*23*).

References and Notes

1. United Nations Environmental Programme (UNEP), *Environmental Effects of Ozone Depletion: 1998 Assessment* (UNEP, Nairobi, Kenya, 1998).
2. D. L. Albritton, P. J. Aucamp, G. Megie, R. T. Watson, Eds., *Scientific Assessment of Ozone Depletion: 1998* (Report No. 44, World Meteorological Organization, Global Ozone Research and Monitoring Project, Geneva, 1998).
3. World Meteorological Organization (WMO), *Scientific Assessment of Ozone Depletion: 1994* (Report No. 37, WMO, Global Ozone Research and Monitoring Project, Geneva, 1995).
4. The ozone measurements are from an assimilation based primarily on ground-based Dobson instruments but supplemented by homogenized data from other sources, including satellite data, when no Dobson measurements are available. B. J. Connor, G. E. Bodeker, R. L. McKenzie, I. S. Boyd, *Geophys. Res. Lett.* **26**, 189 (1999).
5. R. L. McKenzie, in *Ozone in the Troposphere and Stratosphere, Proceedings of the Quadrennial Ozone Symposium 1992*, R. D. Hudson, Ed. (NASA CP-3266, NASA, Greenbelt, MD, 1994), pp. 627–630.
6. A. F. McKinlay and B. L. Diffey, in *Human Exposure to Ultraviolet Radiation: Risks and Regulations*, W. F. Passchier and B. F. M. Bosnajakovic, Eds. (Elsevier, Amsterdam, 1987), pp. 83–87.
7. Sunburning UV radiation, DNA-damaging UV radiation, and plant-damaging UV radiation are three biological weighting functions for UV radiation damage. These functions differ in shape, but in each case, they peak in the UV-B radiation region and decrease with increasing wavelength (and can include the UV-A radiation region). Details of these functions are given in (*6*), (*19*), and (*20*), respectively. The differences in RAF are essentially related to the peak wavelength and the gradient of the functions. Peaks at shorter wavelengths and steeper slopes make them more sensitive to ozone, leading to larger RAFs.
8. R. L. McKenzie, G. E. Bodeker, D. J. Keep, M. Kotkamp, J. H. Evans, *Weather Clim.* **16**, 17 (1996).
9. J. L. Relethford and R. L. McKenzie, *Am. J. Phys. Anthropol.* **107**, 223 (1998).
10. G. Seckmeyer and R. L. McKenzie, *Nature* **359**, 135 (1992).
11. G. Seckmeyer *et al.*, *Geophys. Res. Lett.* **22**, 1889 (1995).
12. J.-L. Bulliard and B. Cox, *N. Z. Public Health Rep.* **3**, 73 (1996).
13. The UV Index represents the integral of the spectrum (watts per square meter per nanometer) weighted by the erythemal action spectrum (*6*) and scaled by 40. The UV Index was originally devised in Canada to give maximum values of around 10 in that country. [WMO, Report of the WMO meeting of experts on UV-B measurements, data quality and standardization of UV indices (WMO, Geneva, 1994)].
14. The sensitivity of UV radiation to ozone change is given by the radiative amplification factor (RAF), which gives the increase expected for each 1% decrease in ozone. Changes were deduced with a simple power law relation between changes in ozone and changes in UV (*13*). The RAF for erythemal UV radiation under these conditions is 1.2. For more detail, see S. Madronich, R. McKenzie, M. M. Caldwell, and L. O. Björn [*Ambio* **24**, 143 (1995)].
15. R. L. McKenzie, P. V. Johnston, M. Kotkamp, A. Bittar, J. D. Hamlin, *Appl. Opt.* **31**, 6501 (1992).
16. B. W. Forgan and J. B. Liley, in *Aerosols and UV in New Zealand, UV Radiation and Its Effects—An Update, Report of a Workshop Sponsored by the National Science Strategy Committee on Climate Change, December 1997* (Miscellaneous Series 49, Royal Society of New Zealand, Wellington, 1997), pp. 51–54.
17. R. L. McKenzie, K. J. Paulin, S. Madronich, *J. Geophys. Res.* **103**, 28785 (1998).
18. K. Stamnes, J. Slusser, M. Bowen, *Appl. Opt.* **30**, 4418 (1991).
19. M. M. Caldwell, L. B. Camp, C. W. Warner, S. D. Flint, in *Stratospheric Ozone Reduction, Solar Ultraviolet Radiation and Plant Life*, R. C. Worrest and M. M. Caldwell, Eds. (Springer-Verlag, Berlin, 1986), pp. 87–111.
20. R. B. Setlow, *Proc. Natl. Acad. Sci. U.S.A.* **71**, 3363 (1974).
21. R. McKenzie, B. Connor, G. Bodeker, data not shown.
22. We also investigated the effect of using several different averaging periods, selected for their significance of UV radiation exposure to the population (for example, a "school-holiday" period of mid-December through January). The pattern of increasing UV radiation is also clear in the data from individual months (Fig. 1B).
23. D. T. Shindell, D. Rind, P. Lonergan, *Nature* **392**, 589 (1998).

24. We thank P. Johnston and M. Kotkamp of NIWA Lauder for technical assistance in developing and operating the UV observation program.

28 May 1999; accepted 11 August 1999

Lower Mantle Lateral Heterogeneity Beneath the Caribbean Sea

Ileana Madalina Tibuleac and Eugene Herrin

Seismic wave reflections from Earth's core recorded at seismic arrays in North America from events in the Caribbean Islands, Venezuela, and the Mid-Atlantic Ridge have observed slownesses more than 64 percent greater than predicted by the IASPEI91 standard Earth model. *P* waves turning in the lowermost mantle beneath the same region also have anomalous slowness. The slowness anomalies are not accompanied by significant travel time residuals and appear to be caused by lateral inhomogeneities in the velocity structure of the lower mantle.

On 1 January 1996, unusual signals (Fig. 1) from an earthquake in the Windward Islands [42.8-degree (*1*) epicentral distance] were recorded at the TXAR (Texas array) seismic array (*2, 3*) in the Big Bend area of west Texas (Fig. 2). Compressional waves reflected from Earth's core (*PcP*) had a much higher amplitude than the direct, first-arriving compressional waves (*P*). Large-amplitude *PcP* waves were also recorded at stations in California, Wyoming, and Canada (*2*). The earthquake was anomalous because the *PcP* slowness magnitude values measured at the TXAR and YKA (Yellowknife, northern Canada) seismic arrays were much larger than predicted by the IASPEI91 seismological tables (*4*). These tables are referred to here as the standard Earth model. Slowness magnitude, referred to subsequently as slowness, is measured as the reciprocal of the horizontal phase velocity and is directly related to the angle of incidence of the arriving ray. It is a measure of the travel time of an arrival across an array.

Here we estimate the slowness of *PcP* and teleseismic *P* wave arrivals using the small-aperture TXAR and YKA arrays. Previous studies at large arrays (aperture >100 km) (*5–7*) and at the YKA array (*8*) did not report large slowness residuals (*9*) for *P* phases, but mislocations were found for ray paths traveling in the deep mantle beneath the northern edge of South America, the Caribbean Sea, and the Gulf of Mexico. Although deep mantle heterogeneities were considered (*5, 8*) to explain the mislocations, these studies concluded (*6–8*) that source region, array site, or upper mantle structure near the arrays were more likely causes. The averaging effect in

Department of Geological Sciences, Southern Methodist University, Dallas, TX 75275–0395, USA. E-mail: (for I.M.T.) ileana@passion.isem.smu.edu; (for E.H.) herrin@passion.isem.smu.edu

the lower mantle on slowness when dealing with a small heterogeneity observed at a large array is similar to the effect of a large heterogeneity observed at a small array. The advantage of smaller arrays is the capability of determining slowness residuals for each ray path and of distinguishing features less than 100 km in dimension.

The database was recorded at Prototype International Data Center (PIDC) between January 1995 and May 1998 for short-period (~1 s) *P* and *PcP* arrivals (*2*). We used data from 107 earthquakes recorded at TXAR and 111 earthquakes recorded at YKA. All events had body wave magnitude (*3*) $m_b \geq 3.5$ and were recorded at more than 10 stations. The sampling rate (*10*) is 20 samples per second for YKA and 40 samples per second for TXAR. We used the cross correlation method (*10, 11*) to refine the frequency wave number (*f-k*) (*3, 10*) data processing at TXAR.

To determine the resolving power of the arrays for measurements of slowness, we used six French explosions almost collocated in the Tuamotu Archipelago (Fig. 2) and observed at TXAR and YKA (Table 1). The resolving power is represented inversely by the sample standard deviation of the slowness estimates, *s* (seconds per degree). The resolving power is about a factor of 2 less for TXAR (s = 0.22) than for YKA (s = 0.08). This is expected because the aperture of YKA (22 km) is about five times that of TXAR (4 km) and the sampling rate at

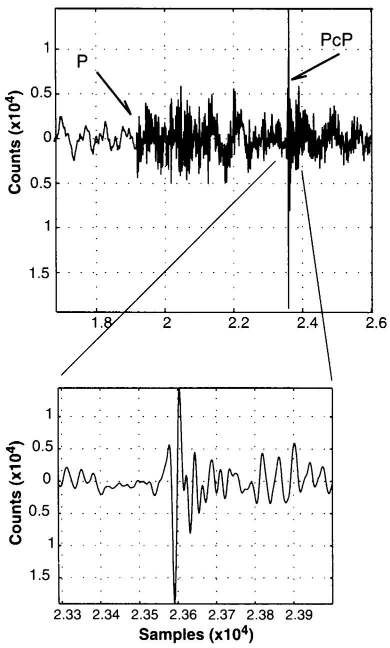

Fig. 1. The vertical component seismogram from one of the TXAR elements, TX07, from the 01/01/1996, 09:38:27 Windward Islands event (m_b = 5.0). The horizontal axis represents time in samples (sample rate is 40 samples per second), and the vertical axis represents velocity amplitude in counts. Both *P* and *PcP* arrivals are marked.

Table 1. Date (day/month/year) and observed *P* slowness values at TXAR and YKA arrays from the French nuclear tests in Tuamotu Archipelago (1995 to 1996). $\bar{x}$, mean slowness; *s*, sample standard deviation.

	Slowness (s/deg.)	
Event date	TXAR	YKA
05/09/1995	9.7	4.2
01/10/1995	9.4	4.4
27/10/1995	9.4	4.4
21/11/1995	9.3	4.3
27/12/1995	9.0	4.4
27/01/1996	9.4	–
$\bar{x}$ (s/deg.)	9.4	4.3
s (s/deg.)	0.22	0.08

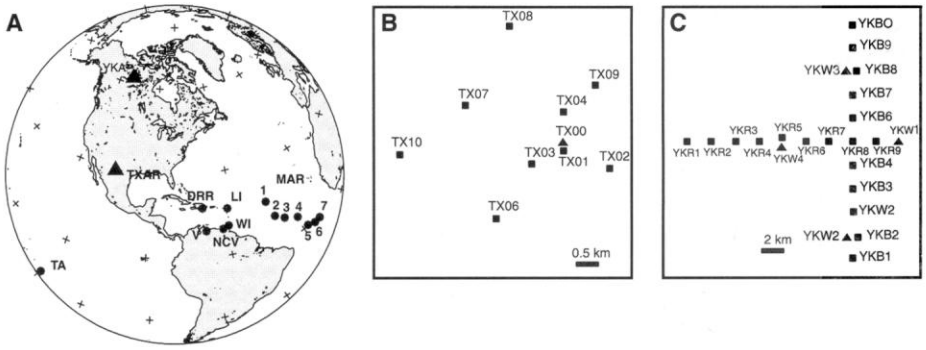

Fig. 2. Locations of the event groups used in this study are represented by black dots in (**A**) and listed as follows: Dominican Republic region (DRR), 18°N, 70°W; Leeward Islands (LI), 17°N, 61°W; Windward Islands (WI), 11°N, 61°W; Venezuela (V), 10°N, 69°W; near coast of Venezuela (NCV), 10°N, 63°W; northern Mid-Atlantic Ridge (MAR 1), 16°N, 46°W; MAR 2, 10°N, 43°W; MAR 3, 8°N, 39°W; MAR 4, 6°N, 33°W; MAR 5, 0.8°N, 28°W; MAR 6, 0°N, 24°W; MAR 7, 0.5°N, 21°W; and Tuamotu Archipelago (TA), 22°S, 139°W. Location of the arrays is represented by black triangles. (**B** and **C**) Configuration and location (black diamonds) of the arrays TXAR (Lajitas, Texas) (B) and YKA (Yellowknife, Canada) (C). Squares represent vertical component seismometers and triangles represent three-component stations. TX00 in (B) is located at 29.4°N, 103.7°W and YKR8 in (C) is located at 62.5°N, 114.6°W.

Table 2. Slowness residuals (ΔS), travel time residuals (ΔTT), and their standard error (SEM) for events at distances up to 85 deg. from TXAR coming from a backazimuth range of 90° to 110° and for events at distances up to 75 deg. from YKA coming from a backazimuth range of 100° to 128°. The abbreviations are as in Fig. 2.

Location	Phase	Median distance (deg.)	Distance range (deg.)	No. of events	Mean ΔS (s/deg.)	SEM ΔS (s/deg.)	Mean ΔTT (s)	SEM ΔTT (s)	Turning depth (km)
				TXAR					
DRR	*P*	32.4	31.2–33.1	12	0.1	0.1	0.4	0.2	800
	PcP	32.1	31.2–32.7	9	2.2	0.2	0.6	0.1	–
LI	*P*	40.6	37.8–42.2	12	0.3	0.1	−0.2	0.2	970
	PcP	40.6	39.1–42.2	9	2.6	0.1	1.4	0.1	–
NCV	*P*	42.5	41.6–43	6	0.4	0.2	1.1	0.3	1020
	PcP	42.5	41.3–43	8	2.3	0.1	0.9	0.3	–
WI	*P*	43.5	41.4–43.8	28	0.2	0.1	−0.1	0.1	1050
	PcP	43.6	42.2–44.4	28	2.3	0.05	1.2	0.2	–
MAR1	*P*	54	53.5–56.3	7	0.1	0.2	−0.2	0.2	1350
	PcP	54	53.5–55.8	6	2.1	0.4	0.4	0.2	–
MAR3	*P*	64	62.7–66.9	7	0.2	0.3	−0.5	0.3	1680
MAR4	*P*	69.1	67.9–71.4	8	0.4	0.2	−0.6	0.2	1870
MAR5	*P*	76.3	75.3–77.4	11	1.4	0.1	−0.8	0.2	2150
MAR6	*P*	80.3	78.4–81.6	8	1.6	0.3	−0.01	0.3	2320
MAR7	*P*	84.3	83.1–85	6	1.2	0.4	−0.4	0.2	2500
				YKA					
DRR	*P*	53.2	51.8–54.3	17	−0.25	0.1	−0.9	0.1	1330
	PcP	52.9	52.5–53.5	4	2.2	0.4	−0.3	0.3	–
LI	*P*	58.0	56–60.5	20	0.5	0.1	−0.7	0.1	1480
	PcP	59.0	57.8–60.1	4	2.5	0.4	−0.5	0.1	–
V	*P*	61.1	60.5–61.7	10	0.2	0.03	−0.6	0.1	1590
WI	*P*	62.7	59.5–64	41	0.7	0.03	−0.8	0.1	1640
	PcP	63.8	63.2–63.8	5	3.2	0.2	−0.5	0.2	–
NCV	*P*	63.5	62.6–64.2	16	0.7	0.05	−0.9	0.2	1670
MAR2	*P*	71.7	68.4–72.8	7	0.4	0.2	−1.1	0.4	1970

TXAR is twice that of YKA. The mean slowness for more than five closely spaced events can be resolved better than 0.2 s/deg. by TXAR and 0.1 s/deg. by YKA; therefore arrays with small aperture can be used to estimate small values of slowness.

We examined TXAR and YKA data (*12*) from the Windward Islands for *P* and *PcP* arrivals for 28 events at TXAR and 41 events at YKA (Table 2). The time and slowness anomalies were considered to be significantly different from zero when the absolute value of their mean was larger than three times the standard error of the mean (*13*). At TXAR, the *P* wave arrivals showed no significant travel time residual. The mean slowness residual was 0.2 s/deg. and was also insignificant considering the resolving power of the array and the standard error (0.1 s/deg.). The *P* wave from Windward Islands to TXAR turns about 1840 km above the core. The *PcP* wave, which traverses the entire mantle and is reflected off of the outer core, has a slightly positive mean travel time residual (1.2 s with a standard error of 0.2 s). The expected slowness for *PcP* at TXAR from the Windward Islands sources is predicted to be 3.4 s/deg. by the standard Earth model. However, the mean of the observed value for the 28 Windward Islands events is 5.7 s/deg. with a standard error of 0.05 s/deg.

YKA data from the Windward Islands events (Table 2) showed negative travel time residuals for *P* and *PcP*, as expected, because of the location of the array on the stable, high-velocity Canadian Shield. For Windward Islands events the mean slowness residual for *P* waves, which turn about 1250 km above the core, was positive (0.7 s/deg.) and significant (standard error 0.03 s/deg.). The expected slowness was 6.6 s/deg. and the observed slowness was 7.3 s/deg. We obtained only five *PcP* slowness values at YKA for this data set, but the mean observed slowness was 7.3 s/deg. (same as the one for *P*), compared with the expected slowness from the standard Earth model of 4.1 s/deg.

Slowness values can also be expressed in terms of the angle of incidence of the arriving ray at the station, with the assumption of a particular crustal structure. The predicted *PcP* incidence angle at TXAR for the Windward Islands events based on the standard Earth model (compressional velocity of 5.0 km/s in the uppermost crust) is 8.8°, but the observed mean value is 14.9°. Likewise, the predicted angle for *PcP* at YKA (compressional velocity of 5.5 km/s in the uppermost crust) is 11.7°, but the observed value is 21.2°.

Using a reciprocal argument, were we to start a compressional ray from TXAR with the incidence angle observed for *PcP* (14.9°) using the standard Earth model, the ray would turn about 750 km above the core. Similarly for YKA, a compressional ray leaving the array with an incidence angle of 21.2° would turn about 1500 km above the core. Thus, according to the standard model, the arrivals we have called *PcP* could not be core reflections, even though the travel times fit within the maximum 1.4 s for *PcP* and the arrivals were systematically identified by PIDC as *PcP*.

We next consider whether the anomalies could be due to shallow structure under the arrays (surface to 60 km depth) or to shallow structure beneath the source (surface to maximum 260 km). On the basis of calibration data from TXAR (*11*), the rays coming from the Windward Islands (106° backazimuth) should have the largest azimuth residuals and negligible slowness residuals. We analyzed events at distances up to 85 deg. from TXAR coming from a backazimuth range of 90° to 110° (Table 2). If *P* waves coming up to the arrays with a slowness comparable to *PcP* slowness and in the same azimuth range do not have slowness residuals significantly different from zero, then we can eliminate the hypothesis of shallow anomalies under the arrays. There are no slowness residuals significantly different from zero for *P* up to 70 deg. epicentral distance from TXAR. *P* waves from sources at distances greater than 70 deg. that turn 740 km above the core beneath the Caribbean Sea begin to have slowness residuals significantly different from zero (Table 2). All *PcP* arrivals up to 54 deg. epicentral distance have large slowness residuals (minimum 2.1 s/deg. with a standard error of 0.4 s/deg. for the Mid-Atlantic Ridge). There were also examples of *P* and *PcP* waves arriving with the same slowness that showed no significant slowness residuals for *P* but did show anomalous *PcP* slowness (Table 3).

Studies of the data recorded at YKA (*8*, *14*) do not suggest any dipping discontinuity or other type of heterogeneity from zero to 60 km beneath the array. At YKA (Table 2) slowness residuals significantly different from zero were observed for events where *P* turned deeper than 1480 km for an azimuth range from 116° to

Table 3. Examples of *P* and *PcP* arrivals at TXAR that have the same observed slowness (slow.) and similar observed backazimuth. The *P* arrivals have no significant slowness anomalies, but all the *PcP* arrivals present large values of slowness residuals (ΔS). *d*, epicentral distance; Obs. baz., observed backazimuth; Obs. slow., observed slowness.

Phase	Date (d/mo/yr)	Origin time (hr:min:s)	*d* (deg.)	Depth (km)	Obs. baz. (°)	Obs. slow. (s/deg.)	ΔS (s/deg.)
P	03/02/1995	06:42:46.2	73	0	109.9	6.8	0.9
PcP	8/12/1995	08:36:45.3	55.75	25.7	109.2	6.8	2.9
P	16/04/1997	13:30:24.2	70.97	0	127	6.3	0.2
PcP	08/04/1997	23:46:18	43.56	37.5	127	6.2	2.8
P	31/07/1996	05:48:23.9	72.51	0	111.3	6.3	0.3
PcP	16/10/1997	08:27:29.9	42.84	64	116	6.2	2.8
P	22/10/1996	10:27:20.1	67.89	0	105.9	6.1	−0.2
PcP	24/09/1995	02:29:11.4	53.54	0	108.5	6.1	2.3
P	02/02/1995	12:53:53.3	59.56	0	119.8	6	−0.9
PcP	08/04/1997	17:11:53.8	43.66	0	120.5	5.9	2.5
P	05/01/1998	01:10:28	71.52	0	112.8	5.9	−0.1
PcP	22/04/1997	10:30:14.3	43.55	0	117.3	5.9	2.4
P	06/01/1998	9:47:04.9	64.96	0	106.7	5.8	−0.7
PcP	22/10/1997	06:30:19.8	53.89	0	113.5	5.7	1.9
PcP	08/04/1997	09:37:42.9	43.65	0	114	5.6	2.3
P	20/02/1998	03:01:05.4	63.52	0	106.3	5.5	−1.1
PcP	02/04/1997	06:14:27.7	43.41	15.7	119.1	5.5	2.1
P	16/04/1997	17:50:22.4	62.15	0	114.4	5.4	−1.2
PcP	25/02/1996	23:20:41.8	43.83	0	114	5.0	1.7
PcP	23/04/1997	10:39:59.5	43.67	0	124.6	5.4	2.0
PcP	19/01/1997	12:44:46	31.25	0	104.8	5.3	2.7
PcP	22/04/1997	10:22:44.7	43.63	0	118.7	5.2	1.8

Table 4. List of the events represented in Fig. 3. *d*, epicentral distance.

Event	Date (d/mo/yr)	Origin time (hr:min:s)	Latitude (deg.)	Longitude (deg.)	Depth (km)	m_b	*d* (deg.)
1	24/04/1996	18:56:23.8	18.8 N	70.3 W	85.1	4.8	32.1
2	24/09/1996	11:42:20.8	15.2 N	61.5 W	152.7	5.5	41.3
3	01/01/1996	09:38:27.9	11.2 N	61.9 W	75.8	5.0	42.8
4	12/05/1996	12:41:40.8	10.6 N	62.2 W	0	4.2	42.9
5	22/04/1997	09:31:13.6	11.1 N	61.0 W	0	5.5	43.6
6	04/05/1997	01:44:53.2	11.1 N	61.1 W	14.6	5.0	43.7
7	28/12/1997	08:36:45.3	13.6 N	45.6 W	25.7	4.7	55.7

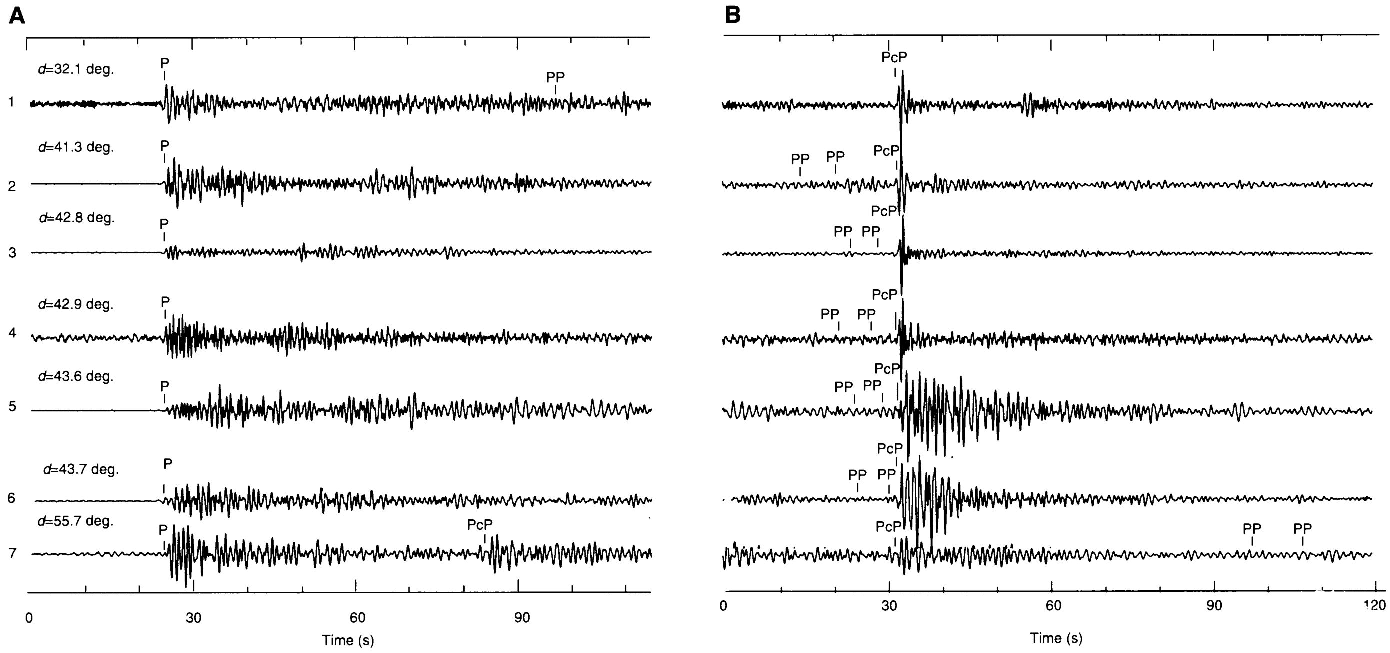

Fig. 3. Example of events in the 90° to 110° backazimuth range from TXAR. The events (labeled 1 to 7) are listed in Table 4, and all had anomalous *PcP* wave slowness. The *f-k* beams of the waveforms filtered between 0.6 and 4.5 Hz using the observed slowness and backazimuth for the *PcP* arrivals are presented. The waveforms are aligned on the observed *P* arrivals in (**A**) and on the observed *PcP* arrivals in (**B**). *PP* predicted arrival times are also marked for each epicentral distance (*d*).

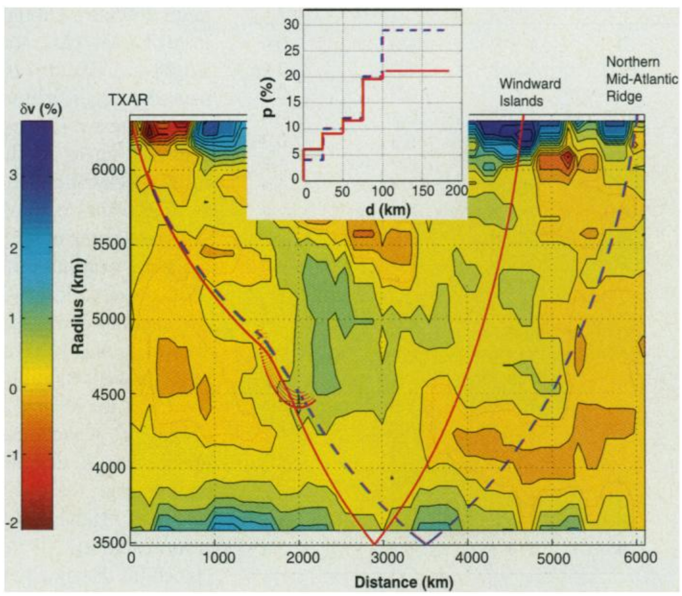

Fig. 4. The *PcP* ray paths resulting from the model from Windward Islands (red continuous line) and from the northern Mid-Atlantic Ridge (blue dashed line). In the inset the variation of the velocity increase *p* for each ray is represented as a function of the distance *d* inside the first ellipse. The distance between successive ellipses was chosen to be 25 km. The background represents for comparison a slice (at 106° backazimuth from TXAR) through Grand's (*16*) shear wave velocity anomaly (δ*v*) model.

Table 5. Results of ray tracing at TXAR through the elliptical velocity anomalies model. Calculated travel time (Calc. TT) and epicentral distance (Calc. *d*) are compared with the table travel time and the median epicentral distance for *PcP* arrivals from events in Windward Islands (WI) and the northern Mid-Atlantic Ridge (MAR1). The values of the velocity anomalies added to the IASPI91 radial velocity model in each ellipse are noted as p1 to p5. Obs. slow., observed slowness.

Location	Phase	Obs. slow. (s/deg.)	Table TT (s)	Median *d* (deg.)	Calc. TT (s)	Calc. *d* (deg.)	Velocity anomalies (%)				
							p1	p2	p3	p4	p5
WI	*PcP*	5.7	594.1	43.4	594.9	42	6	9	11.5	19.5	21
MAR1	*PcP*	5.94	631.2	53.9	631.4	54.1	4	10	12	20	29

125°. Important exceptions were the events in Venezuela (127° backazimuth) and the Mid-Atlantic Ridge (100° backazimuth) whose *P* wave arrivals did not have slowness residuals significantly different from zero, even though the *P* waves turned below 1600-km depth in the mantle. These results indicate that those *P* rays are not passing through an anomalous region. All *PcP* slowness residuals from the Dominican Republic region, Windward Islands, and Leeward Islands were more than 2.1 s/deg. at YKA. Thus, the anomalous slowness residuals were observed for *PcP* and deep mantle *P* waves but not for *P* waves from events up to 76 deg. from TXAR. Significant slowness anomalies of *PcP* waves and some of the deep mantle *P* waves were also observed at YKA. These observations suggest that the cause of the anomalies is in a region within 1300 km of the core-mantle boundary and is not due to shallow structure under the arrays.

The range of depths for events from different locations was 0 to 260 km (*15*). We eliminated the possibility of structural difference in the source region to be the cause of these slowness anomalies because we saw similar anomalies for shallower and deeper earthquakes. Thus, events from different locations and at different depths around the Caribbean Sea show similar slowness anomalies for *PcP* at both arrays, indicating that structure beneath the source is not the cause of the observed anomalies.

For epicentral distances between 42 and 44 deg., the standard Earth model predicts a minimum ~0.7 s and maximum ~10 s arrival time difference between the *PP* and *PcP* phases. The anomalies are not due to interference between these phases (see Fig. 3 and Table 4) because, for each event, the *f-k* beam of the waveforms filtered between 0.6 to 4.5 Hz using estimated *PcP* slowness and backazimuth shows a very distinct *PcP* arrival and *PP* arrivals are weak if they are observed. Therefore we eliminated the possibility of interference of *PP* with *PcP* arrivals.

The hypothesis of velocity anomalies in the lower mantle beneath the Gulf of Mexico and the Caribbean Sea is supported by tomographic models for compressional and shear waves (*16–19*). Nonradial velocity gradients associated with the structures delineated by the tomographic models would be expected to produce refractions that could lead to the anomalous slowness residuals we observed. Whereas the travel time anomalies found by tomographic models are of the order of several parts per thousand relative to total travel times, the slowness anomalies described here are more than 64% larger than the values given by the standard Earth model. Furthermore, the estimates of these anomalies are independent of errors in estimated origin time of earthquakes and are only marginally (±0.1 s/deg.) affected by errors in the estimated hypocenter.

We built a simple test model to determine what velocity gradient would be required to obtain the observed slowness anomalies with the observed travel time residuals. We observed the location and dimensions of shear wave velocity anomalies inferred by tomographic models (*16*, *17*). A slice at 106° backazimuth from TXAR in Grand's (*16, 17*) shear wave model has a high-velocity, almost vertical feature at ~20 deg. from TXAR from 1500- to 1900-km depth (see in Fig. 4 the background and the color bar for values of shear velocity anomaly δv). *PcP* rays at TXAR pass through the lower edge of this feature toward the array. We also observed that *PcP* and deep mantle *P* phases at TXAR seem to be focused in a narrow slowness range, as if deviated by a velocity anomaly similar to a lens in that region. We chose elliptical layers to represent the geometry similar to the variations in the tomographic velocity anomalies between 1500- and 1900-km depth. We imagined the nonradial velocity layers between 1500- and 1900-km depth as the lower part of five superposed concentric ellipses in which a constant increase in velocity (p) is added at each depth to the IASPI91 model of radial velocity variation. In Table 5 the velocity increases in percents are labeled p1 to p5. The location of the center of the ellipses was chosen to be 2000 km from TXAR and at 1320-km depth. This depth is close to the center of the fast anomaly in Grand's model. The larger ellipse has a 1300-km vertical axis and 1000-km horizontal axis.

Using our model, we considered individual rays that were representative of each group of events (Table 2). Ray tracing was performed starting at the TXAR array with the observed slowness, looking for the combination of anomalies in each ellipse that would bend the *PcP* rays but maintain travel times. Table 5 presents the results of ray tracing for *PcP* from Windward Islands and the northern Mid-Atlantic Ridge at TXAR. The *PcP* ray paths resulting from the model are presented in Fig. 4. On the same figure the variation of the velocity increase p (in percent) is represented in each ellipse as a function of the distance d (kilometers) inside the first ellipse. The model delineates a structure dipping to the southeast of ~600 km in length and ~125 km wide, located at the boundary of the fast region found with shear wave tomography and presented in the background in Fig. 4 for comparison. The largest velocity anomaly added to the standard Earth model velocity to obtain the necessary bending of the rays and match the observed travel times for the Windward Islands events was 21% for 25-km distance between the ellipses. The largest velocity anomaly to be added was 29% in the case of the northern Mid-Atlantic Ridge events. The results are dependent on the geometry of the model and should only be considered a first approximation. The reason we chose an elliptical geometry to describe the anomalies was the shape of the tomographic fast anomaly and the simplicity of the calculations.

So far velocity heterogeneities of only several percent with lateral scale lengths of several hundred kilometers in Earth's mid-mantle and lowermost mantle have been calculated with tomographic models (*16, 17, 19, 20*). Recently it was found that anomalies in the lowermost ~100 kilometers of the mantle (*21–24*) could be much larger (reductions of 10% or more in *P* and up to 30% reductions in *S* velocities). One of the problems of the existing global tomographic models (*19–21*) is that they are the result of damped least squares inversions that underestimate the anomalous velocity gradients and overestimate the width of the heterogeneity. It seems that larger velocity anomalies are possible in confined zones that affect the travel time of *P* waves (by as much as 1.4 s) and cause the waves to be deflected from their normal path. These anomalies could be the expression of the nonradial velocity gradients associated with the transition between the cold downwellings supposed to be old subducted ocean crust (*16*) and the rest of the lower mantle, or they could be an expression of topography at the boundary between compositionally distinct regions at a depth of about 1600 km predicted by recent models of the mantle (*25, 26*).

References and Notes

1. We use the notation "deg." for epicentral distance units and the degree sign (°) for degrees of azimuth or angle of incidence. One deg. is equivalent to ~111.2 km.
2. A seismic array is a set of sensors (seismometers) distributed over an area of Earth's surface at spacing narrow enough so that the signal may be correlated across the array (*3*). The data used in our analysis and further information about the arrays are available at http://www.pidc.org/dataprodbox/prod.html
3. K. Aki and P. G. Richards, *Quantitative Seismology, Theory and Methods* (Freeman, San Francisco, 1980).
4. B. L. N. Kennett, Ed., *IASPEI 1991 Seismological Tables* (Research School of Earth Sciences, Australian National University, Canberra, Australia, 1991). IASPEI is the International Association of Seismology and Physics of the Earth's Interior.
5. C. Powell, *Nature*, **254**, 40 (1973).
6. L. J. Burdick and C. Powell, *J. Geophys. Res.* **85**, 3485 (1980).
7. L. R. Johnson, *Bull. Seis. Soc. Am.* **59** 973 (1969).
8. C. Wright, *J. Geophys. Res.* **78**, 4965 (1973).
9. A residual is the difference between the observed value and the value predicted by the standard Earth model.
10. The seismogram is digitized at discrete time points. The number of points equally spaced in time recorded in a second is the sampling rate. Estimates of the horizontal velocity across the array are obtained either from the best beam with the *f-k* method (*3*) or from the relative time delays between the arrivals at the array stations with the cross correlation method. More data samples (higher sample rate) mean better constrained waveform shape, that is, better constrained relative time delays (or beams) and enhanced capability of the array to estimate high values of the horizontal phase velocity. Data processing at TXAR (*11*) includes Fourier interpolation up to 320 samples per second.
11. I. Tibuleac and E. Herrin, *Seism. Res. Lett.* **68**, 353 (1997). The M discontinuity beneath TXAR was determined to the first order to strike along an azimuth of 109° (NW-SE) and dip 11° to the northeast. The rays coming along the strike have maximum azimuth residual and minimum slowness residual.
12. Data from TXAR were obtained from Southern Methodist University Geophysics Laboratory archives and reprocessed for all events. Estimates for YKA are from the *Reviewed Event Bulletins* of the PIDC (*2*).
13. The standard error of the mean (referred to here as the standard error) is the ratio of the sample standard deviation and the square root of the number of events.
14. K. Koch and U. Kradolfer, *Bull Seismol. Soc. Am.* **87**, 1576 (1997).
15. The location and depth range of events are as follows: Dominican Republic region, 0 to 160 km; Leeward Islands, 0 to 230 km; Windward Islands, 0 to 260 km; Venezuela, 0 to 180 km; near coast of Venezuela, 0 to 180 km; and Mid-Atlantic Ridge, 0 to 40 km.
16. S. P. Grand, R. Van der Hilst, S. Widiyantoro, *GSA Today* **7**, 1 (1997).
17. S. P. Grand, *J. Geophys. Res.* **99**, 11591 (1994).
18. R. J. Pulliam, D. W. Vasco, L. R. Johnson, *ibid.* **98**, 699 (1993).
19. R. D. Van der Hilst, S. Widiyantoro, E. R. Engdahl, *Nature* **386**, 578 (1997).
20. X.-F. Liu, J. Tromp, A. M. Dziewonski, *Earth Planet. Sci. Lett.* **160**, 343 (1998).
21. T. Lay, Q. Williams, E. J. Garnero, *Nature* **392**, 461 (1998).
22. L. Wen and D. V. Helmberger, *Science* **279**, 1701 (1998).
23. D. V. Helmberger, L. Wen, X. Ding, *Nature* **396**, 251 (1998).
24. Q. Williams and E. J. Garnero, *Science* **273**, 1528 (1996).
25. L. H. Kellogg, B. H. Hager, R. D. Van der Hilst, *ibid.* **283**, 1881 (1999).
26. R. D. Van der Hilst and H. Kárason, *ibid.*, p. 1885.

27. We thank S. Grand for fruitful discussions and B. Stump, D. Blackwell, J. Bonner, C. Hayward, M. Sorrells, and R. Gregory for helpful comments and review of the manuscript. Supported by grant 01-97-1-0024 from the Defense Special Weapons Agency.

14 June 1999; accepted 15 July 1999